FACTA UNIVERSITATIS
Series: **Mechanical Engineering** Vol. 3, N° 1, 2005, pp. 41 - 57

PERFORMANCE PREDICTION OF HYDRAULIC TURBOMACHINERY

UDC 539.421:519.711

Nebojša Jovičić, Milun Babić, Gordana Jovičić, Dušan Gordić

University of Kragujevac, Faculty of Mechanical Engineering,
Sestre Janjića 6, 34000 Kragujevac, Serbia&Montenegro

Abstract. *In this paper an accurate and efficient numerical algorithm for simulation of three-dimensional turbomachinery flows is presented. This model is used later for turbomachinery performance prediction. Mathematical model is based on the RANS equations that are written in non-inertial frame of reference. Reynolds stresses are approximated with Boussinesq hypothesis using two-equation k-ω near-wall turbulence closure. Discretization of convective fluxes of the mean flow equation is performed using central differences, by explicitly added eigenvalue scaling non-isotropic matrix-valued artificial dissipation. In turbulence closure equations, numerical convective fluxes are approximated according to Roe second order upwind scheme in conjunction with monotone (TVD) variable extrapolations. The semi-discrete equations are advanced in time using a four stage explicit Runge-Kutta scheme enhanced with local time stepping, variable coefficient implicit residual smoothing and multigrid acceleration. Developed software is applied for numerical analysis of work processes in the model of NEL mixed-flow bowl pump. Obtained numerical results are in good agreement with the available experimental data in the operating conditions at the best efficiency point (BEP). Also, turbopump performances are simulated for number flow rates and constant shaft speed, corresponding to the off-design operating conditions. According to information from numerical experiment, methodology for design performance characteristics is shown. By further improvement of mathematical model, the developed methodology enables that, from an engineer's perspective, numerical experiment could be a useful, low-cost tool in comparison with the expensive measurements. Using the dimensionless characteristics as well as theory of conformity, the turbopump performance can be calculated within the wide operating regimes in a relatively simple way.*

Key Words: *Numerical Method, RANS, Mixed-flow Pump, Performance Characteristic*

Received January 25, 2005

1. INTRODUCTION

Advances in computing resources account for the fact that the recent trend in Computational Fluid Dynamics is to predict practical engineering problems by solving Navier-Stokes equations with high resolution schemes. An incompressible turbulent flow through turbomachinery impeller is probably one of the most challenging problems in CFD. The numerical simulation of high *Re* number turbulent flows, occurring in complex geometry from the inlet to the exit of hydraulic turbomachinery, requires both a very large number of grid points and extremely small grid spacing in order to resolve phenomena in the near-wall region. Such meshes can dramatically deteriorate the convergence rate of numerical procedure. In order to make an accurate, efficient and low-cost code for engineering purpose, it is very desirable to apply acceleration techniques. Among the acceleration techniques, the multigrid method is said to be the most efficient and general technique known today [1].

The advantage of the multigrid method over the other acceleration techniques is the fact that the rate of convergence is independent of the size of the system to be solved. With much success, the multigrid method has been applied in CFD applications, both compressible [2,3] and incompressible [4,5,6]. The multistage Runge-Kutta scheme, developed by Jameson [7], in conjunction with local time stepping, implicit residual smoothing and the multigrid method is a powerful tool for solving turbomachinery flow problems [8,9,10,11].

In this paper an incompressible multigrid three-dimensional Reynolds-Averaged Navier-Stokes code for analysis of the turbomachinery blade rows and other internal flows is presented. This code is extension of 3D compressible Euler code developed by J. V. Soulis [12]. The application of the 3D incompressible turbulent flow computation, in the NEL mixed-flow bowl pump blade passages, is described and compared to the experimental data [13]. The information from numerical experiment, and the appropriate methodology for design performance characteristics (head, powers, and efficiency in terms of flow rates), presented here, are coupled in order to make a useful tool for high performance turbomachinery design.

2. GOVERNING EQUATIONS

For mathematical modeling of viscous fluid flow in turbomachinery passages, full three- dimensional unsteady Reynolds-averaged Navier-Stokes equations are written first in Descartes coordinate system (x_1, x_2, x_3) rotating with constant angular velocity Ω about x_1 – axis. The rotation introduces source terms in x_2 – and x_3 –momentum equations related to centrifugal and Coriolis forces. Chorin's artificial compressibility formulation [14] is used to obtain coupling of velocity and pressure fields. Due to complex geometry in curved passages, the conservation forms of governing Descartes equation, based on primitive variables, are mapped to a general body-fitted (ξ_1, ξ_2 , ξ_3) coordinate system using standard techniques. An artificial compressibility form of three-dimensional incompressible mean flow equations, non-dimensionalized by the fluid density, reference velocity and reference length, in curvilinear coordinates may be written in tensor notation [4, 15], where repeated indices imply summation, as:

$$\frac{1}{J}\frac{\partial \mathbf{Q}_f}{\partial t}+\frac{\partial}{\partial \xi^j}(\overline{\mathbf{F}}_f^j-\overline{\mathbf{F}}_{fv}^j)=\overline{\mathbf{S}}_f, j=\overline{1,3} \tag{1}$$

In the above equation, J represents Jacobian of geometrical transformation, while vectors $\mathbf{Q}_f$, $\overline{\mathbf{F}}_f^j$, $\overline{\mathbf{F}}_{fv}^j$ and $\overline{\mathbf{S}}_f$ are defined as follows:

$$\mathbf{Q}_f=[P,u_1,u_2,u_3]^T, \tag{2}$$

$$\overline{\mathbf{F}}_f^j=\frac{1}{J}[\beta U^j,u_1U^j+P\xi_{x_1}^j,u_2U^j+P\xi_{x_2}^j,u_3U^j+P\xi_{x_3}^j]^T, j,m=(\overline{1,3}), \tag{3}$$

$$\overline{\mathbf{F}}_{fv}^j=\frac{1}{J}(\frac{1}{\mathrm{Re}}+\nu_t)[0,g^{mj}\frac{\partial u_1}{\partial \xi^m}+R_{m1}\xi_{x_m}^j,g^{mj}\frac{\partial u_2}{\partial \xi^m}+R_{m2}\xi_{x_m}^j,g^{mj}\frac{\partial u_3}{\partial \xi^m}+R_{m3}\xi_{x_m}^j]^T, \tag{4}$$

$$S_f=\frac{1}{J}[0,0,\Omega(\Omega x_2+2u_3),\Omega(\Omega x_3-2u_2)]^T, \tag{5}$$

where P is defined as $p + (2 / 3)k$, p is pressure, k is turbulent kinetic energy, u_i are Descartes velocity components, $\xi_{x_j}^i$ are metrics of transformation, U^i are contravariant velocity components, g^{ij} are components of contravariant metric tensor, and tensor R_{ij} is defined as follows:

$$R_{ij}=\frac{\partial u_i}{\partial \xi^k}\xi_{x_j}^k, \tag{6}$$

In the equation (4) Re is Reynolds number and ν_t is eddy viscosity. For turbulence closure, two-equation $k-\omega$ near-wall model [16] is employed and eddy viscosity is expressed in terms of turbulent kinetic energy k and specific dissipation rate ω. In curvilinear coordinates, equations of turbulence model may be written as [17]:

$$\frac{1}{J}\frac{\partial \mathbf{Q}_t}{\partial t}+\frac{\partial}{\partial \xi^j}(\overline{\mathbf{F}}_t^j-\overline{\mathbf{F}}_{tv}^j)=\mathbf{S}_t, \quad (j=\overline{1,3}), \tag{7}$$

where vectors $\mathbf{Q}_t$, $\overline{\mathbf{F}}_t^j$, $\overline{\mathbf{F}}_{tv}^j$, $\overline{\mathbf{S}}_t$ are defined as follows:

$$\mathbf{Q}_t=[k,\omega]^T, \tag{8}$$

$$\overline{\mathbf{F}}_t^j=\frac{U^j}{J}[k,\omega]^T, \tag{9}$$

$$\overline{\mathbf{F}}_{tv}^j=\frac{1}{J}[(\frac{1}{\mathrm{Re}}+\sigma^*\nu_t)g^{mj}\frac{\partial k}{\partial \xi^m},(\frac{1}{\mathrm{Re}}+\sigma\nu_t)g^{mj}\frac{\partial \omega}{\partial \xi^m}]^T, \tag{10}$$

$$\overline{\mathbf{S}}_t=\frac{1}{J}[P_k-\beta_k k\omega,\ \alpha\frac{\omega}{k}P_k-\beta_\omega\omega^2]. \tag{11}$$

Production of turbulence kinetic energy P_k expressed in terms of tensor R_{ij} (6) is:

$$P_k = \nu_t (R_{ij} + R_{ji}) R_{ij} \,. \tag{12}$$

and eddy viscosity is given as:

$$\nu_t = \alpha^* \frac{k}{\omega} \,. \tag{13}$$

In the equations of turbulence model, $\alpha^*, \alpha, \beta_\omega, \beta_k, \sigma, \sigma^*$ are closure coefficients [16].

3. NUMERICAL METHOD

The governing equations are discretized in space using cell vertex finite volume method. The viscous fluxes at the cell face are approximated with central differencing. Discretization of the convective fluxes of the mean flow equations is performed using central differences, by explicitly added eigenvalue scaling non-isotropic matrix-valued artificial dissipation [17]. At the cell face i+1/2 artificial dissipation flux can be written as:

$$\mathbf{D}^1_{(i+1/2,j,k)} = \varepsilon_{CDM} \left| \mathbf{A}^1 \right| \delta_{\xi^1} \delta_{\xi^1 \xi^1} \widetilde{\mathbf{Q}}_{f(i+1/2,j,k)} \,. \tag{14}$$

where ε_{CDM} is positive constant which controls the amount of artificial dissipation introduced into numerical solution, $\widetilde{\mathbf{Q}}_f$ is variable vector normalized by J, δ_{ξ^j} is central difference operator, $\delta_{\xi^j \xi^j} = \delta^-_{\xi^j} \delta^+_{\xi^j}$ and $|\mathbf{A}^1|$ is absolute value of the Jacobian matrix of convective flux. The convective fluxes of turbulence closure equations, at the cell face i + ½, are formed using Roe-scheme [1]:

$$\widetilde{\mathbf{F}}^1_{t(i+1/2,j,k)} = \frac{1}{2} (\overline{\mathbf{F}}^1_t (\widetilde{\mathbf{Q}}^R_{t(i+1/2,j,k)}) + \overline{\mathbf{F}}^1_t (\widetilde{\mathbf{Q}}^L_{t(i+1/2,j,k)})) -$$

$$\frac{1}{2} [\left| \mathbf{A}^1_{t(i+1/2,j,k)} \right|] (\widetilde{\mathbf{Q}}^R_{t(i+1/2,j,k} - \widetilde{\mathbf{Q}}^L_{t(i+1/2,j,k)}) \,. \tag{15}$$

where $\widetilde{\mathbf{Q}}^R_{t(i+1/2,j,k)}$ and $\widetilde{\mathbf{Q}}^L_{t(i+1/2,j,k)}$ are interface values extrapolated from right and left sides. Interface values can be written in form of monotone variable extrapolation as:

$$\widetilde{\mathbf{Q}}^R_{t(i+1/2,j,k)} = \widetilde{\mathbf{Q}}_{t(i+1,j,k)} - \frac{1}{2} \psi^R_{(i+1/2,j,k)} (\widetilde{\mathbf{Q}}_{t(i+2,j,k)} - \widetilde{\mathbf{Q}}_{t(i+1,j,k)}) \,. \tag{16}$$

$$\widetilde{\mathbf{Q}}^L_{t(i+1/2,j,k)} = \widetilde{\mathbf{Q}}_{t(i,j,k)} + \frac{1}{2} \psi^L_{(i+1/2,j,k)} (\widetilde{\mathbf{Q}}_{t(i,j,k)} - \widetilde{\mathbf{Q}}_{t(i-1,j,k)}) \,. \tag{17}$$

where ψ (**r**) is slope limiter which is a function of consecutive gradients of the solution:

$$\widetilde{\mathbf{r}}^R_{(i+1/2,j,k)} = \frac{\widetilde{\mathbf{Q}}_{t(i+1,j,k)} - \widetilde{\mathbf{Q}}_{t(i,j,k)}}{\widetilde{\mathbf{Q}}_{t(i+2,j,k)} - \widetilde{\mathbf{Q}}_{t(i+1,j,k)}} \,, \quad \widetilde{\mathbf{r}}^L_{(i+1/2,j,k)} = \frac{\widetilde{\mathbf{Q}}_{t(i+1,j,k)} - \widetilde{\mathbf{Q}}_{t(i,j,k)}}{\widetilde{\mathbf{Q}}_{t(i,j,k)} - \widetilde{\mathbf{Q}}_{t(i-1,j,k)}} \,. \tag{18}$$

Slope limiter is introduced in a variable extrapolation in order to avoid numerical problems related to extremely high gradients which turbulence quantities reach in near-wall regions. Differentiable R-κ limiter [18]:

$$\psi(\mathbf{r}) = [(1+\kappa)\mathbf{r}+(1-\kappa)]\frac{\mathbf{r}+|\mathbf{r}|}{(1+\mathbf{r})^2} \quad 0<\kappa<1\,. \tag{19}$$

is implemented and $\kappa = 2/3$ ensure third order of accuracy. The above limiter has a property that for $\mathbf{r} \to \infty$, $\psi(\mathbf{r}) \to 2(1+\kappa)$and in extreme, where $\mathbf{r} < 0$, $\psi(\mathbf{r}) = 0$ leading to extrapolation with first order of accuracy.

The system of the differential equations is advanced in time using an explicit four stage Runge-Kutta scheme until the steady-state solution is reached. For economy, viscous terms are evaluated only at the first stage and then unchanging used for the remaining stages. Artificial dissipative terms are evaluated at the first and second stage [8]. Runge-Kutta scheme can be explained as:

$$\mathbf{Q}^{(p)} = \mathbf{Q}^{(n)} - \alpha_p \Delta t\, J(\mathbf{C}^{(p-1)} - \mathbf{V}^{(1)} - \mathbf{AD}^{(k)} + \mathbf{S}^{(p-1)})\,. \tag{20}$$

where $\mathbf{Q}^{(1)} \equiv \mathbf{Q}^{(n)}$ and $\mathbf{Q}^{(4)} \equiv \mathbf{Q}^{(n+1)}$, p is number of Runge-Kutta stages, n denotes the current time level, α_p are multistage coefficients, Δt is the pseudo-time increment and $k = 1$ for $p = 1$ and k = 2 for p = 2, 3, 4. In the equation (20) **C, V, AD** and **S** represent discrete approximation of the convective, viscous, artificial dissipation and source terms, respectively.

In order to reduce the computational cost, local time-stepping, implicit residual smoothing and multigrid are employed to speed up convergence to the steady-state solutions.

Local time step limit Δt is computed with scaled spectral radii of the flux Jacobian matrices for the convective terms. The time step at every grid point is calculated as:

$$\Delta t_{i,j,k} = \frac{CFL}{\lambda_{\xi^1} + \lambda_{\xi^2} + \lambda_{\xi^3}}\,. \tag{21}$$

where λ_{ξ^i} are the spectral radii of the Jacobian matrices, given as:

$$\lambda_{\xi^i} = \left|U^i\right| + \sqrt{(U^i)^2 + \beta g^{ii}}\,. \tag{22}$$

An implicit smoothing of residuals [19] is used to extend the stability limit and robustness of the basic scheme. This procedure in 3D can be defined as:

$$(1-\varepsilon_{\xi^1}\nabla_{\xi^1}\Delta_{\xi^1})(1-\varepsilon_{\xi^2}\nabla_{\xi^2}\Delta_{\xi^2})(1-\varepsilon_{\xi^3}\nabla_{\xi^3}\Delta_{\xi^3})\,\widetilde{R} = R \tag{23}$$

where residual R includes the contribution of the variable time step and $\widetilde{R}$ is residual after a sequence of smoothing in all three directions. Variable coefficients ε depend on spectral radii of the flux Jacobian matrices as well as Courant numbers of the smoothed and unsmoothed scheme [20]. Hence,

$$\beta_{\xi^i}=\max\{0,\frac{1}{4}[(\frac{CFL}{CFL^*}\frac{\lambda_{\xi^i}}{\lambda_{\xi^1}+\lambda_{\xi^2}+\lambda_{\xi^3}}\Phi_{\xi^i})^2-1]\}\,. \tag{24}$$

$$\Phi_{\xi^i}=1+(\frac{\lambda_{\xi^j}}{\lambda_{\xi^i}})^{\sigma}+(\frac{\lambda_{\xi^k}}{\lambda_{\xi^i}})^{\sigma},\ \ i,j,k=1,2,3;\quad \sigma=0.5, \tag{25}$$

where repeated indices in Eq. (24) and (25) imply no summation.

A nonlinear FAS (Full Approximation Storage) multigrid is used to accelerate the convergence of the explicit four stage Runge-Kutta scheme. Multigrid process starts on the finest grid with grid size *h*. The coarser grids can be created by doubling the grid spacing along three (full-coarsening) or two direction (semi-coarsening). This implies that the grid sizes are 2*h,* 4*h,* etc. After one or more Runge-Kutta time steps a new solution ($\mathbf{Q}_h^{n+1}=\mathbf{Q}_h^4$) results. Using this solution a new residual ($\mathbf{R}_h(\mathbf{Q}_h^{n+1})$ is calculated. In order to improve the solution on the fine grid with aid of a coarse grids, the following steps are carried out [3].

a) Transfer of the solution and the residual to the coarser grid. In the case of the cell vertex scheme the solution on the coarse grid is stored at the grid points corresponding to every second grid point of the fine grid. The fine grid solution can be transferred to the coarser grid using injection:

$$\mathbf{Q}_{2h}^n=\mathbf{Q}_h^{n+1}\,. \tag{26}$$

For transferring the new residual ($\mathbf{R}_h(\mathbf{Q}_h^{n+1})$ to coarser grid full weighting operator ($T_{2h,h}^R$) is employed. The residual from the fine grid is needed on the coarser grid in order to retain the spatial accuracy of the fine grid. For this purpose, one can define a source term "forcing function" as follows:

$$\wp_{2h}=T_{2h,h}^R\mathbf{R}_h(\mathbf{Q}_h^{n+1})-\mathbf{R}_{2h}(\mathbf{R}_{2h}^n)\,. \tag{27}$$

b) Calculation of the new solution on the coarser grid. On the coarser grid, a new solution is obtained in a similar way as on a fine grid. The only change is that forcing function $\wp_{2h}$ is now added to the residual. Hence,

$$(\mathbf{R}^*)_{2h}^p=\mathbf{R}_{2h}(\mathbf{Q}_{2h}^p)+\wp_{2h}\,. \tag{28}$$

c) Interpolation from the coarser to the fine grid. Once the coarsest grid is reached, the accumulated corrections are transferred back to the finest grid using a series of trilinear interpolations on successively finer grids [1]. Then, the new solution on the finest grid becomes:

$$\mathbf{Q}_h^+=\mathbf{Q}_h^{n+1}+T_{h,2h}^C\Delta\mathbf{Q}_{2h}\,, \tag{29}$$

where $\Delta\mathbf{Q}_{2h}$ is correction from coarser grid containing accumulated correction from other coarser grids (4*h,* 8*h,*...). Interpolations of the correction introduce high frequency errors which have to be prevented by using constant coefficient implicit correction smoothing operator before updating solution on the finer grid. Through numerical experiments values $\varepsilon_{\xi^1}=\varepsilon_{\xi^2}=\varepsilon_{\xi^3}$ of (0.8 ÷ 1) are considered to be nearly optimal. On each grid, the

boundary conditions are treated in the same way and updated at every Runge-Kutta step. A three level V-cycle multigrid algorithm with semi-coarsening in the transverse plane is applied only to the mean flow equations with one, two and three iterations performed on the first, second and third grid level, respectively. The turbulence closure equations are solved only on the finest mesh and eddy viscosity is injected to the coarser meshes and kept frozen during the multigrid process. Three single-grid iterations are performed on the turbulence closure equations per multigrid cycle.

In turbomachine channel calculations we had four different types of boundary conditions: inlet, outlet, solid walls and periodicity. Boundary conditions are specified at the inlet and outlet according to the theory of characteristics. At the inlet, in cross-section A_1, (Fig. 1), velocity components, turbulent kinetic energy (k) and specific dissipation rate (ω) are prescribed and pressure is extrapolated from the interior of the domain.

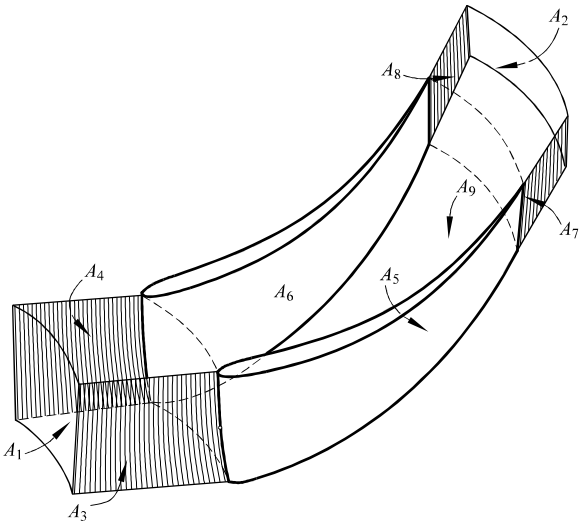

Fig. 1. Impeller Blade Passage

At outlet A_2, pressure at the hub is prescribed and radial equilibrium equation is used to determine the spanwise distribution of the pressure. Velocity components, turbulent kinetic energy (k) and specific dissipation rate (ω), at the outlet, are determined in manner of extrapolation. On solid walls, suction side (A_5), pressure side (A_6) and hub and shroud (A_9) no-slip condition is used as well as two-point extrapolation formula to compute pressure. Turbulent kinetic energy is set to zero at solid walls. The specific dissipation rate at the solid walls, following Menter [21], is calculated as:

$$\omega_W = \frac{60}{\beta_\omega \, \mathrm{Re} \, n_1^2}, \tag{30}$$

where n_1 is minimal normal distance of the first grid node to the solid wall. If the rotating frame of reference is employed, the stationary walls in the inertial frame are treated as moving walls with the rotation velocity of the frame in the reverse direction. Periodicity at

the inlet (A_3 and A_4) and outlet (A_7 and A_8) from one blade passage to another is obtained by using virtual cells.

4. APPLICATIONS

The method described above is implemented in three-dimensional RANS solver and applied to numerical analysis of work processes in the model of mixed-flow pump.

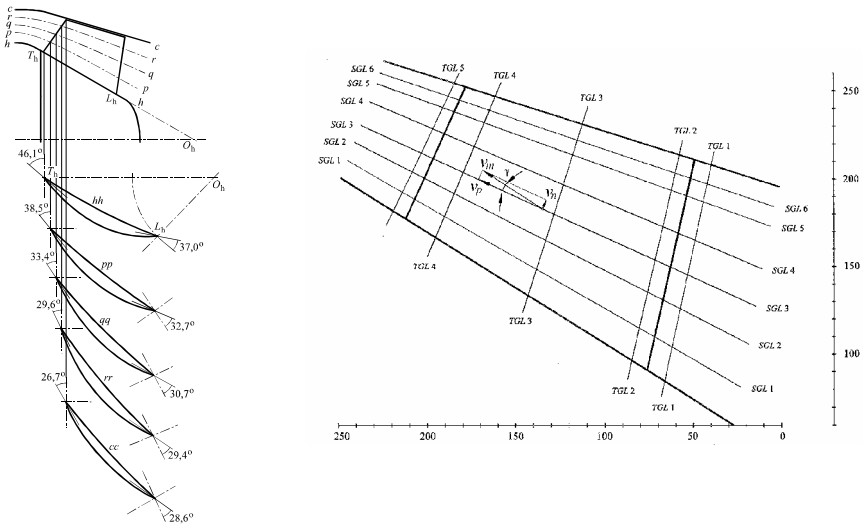

a) b)

Fig. 2. a) Impeller Blade Profiles Showing Inlet and Outlet Angles,
b) Meridian Section through Pump Showing Measuring Station Position

The obtained results are compared to the experimental data obtained by using the Laser Doppler Anemometry method [22]. The experiment is done at the National Engineering Laboratory in Glasgow, UK. The experimental pump is with five blades mounted on a conical hub, without stator, so that the working fluid is approaching the impeller without circular velocity component. Both the hub and casing have a cone shape with semiangles 32,3° and 17,6° respectively. The impeller outlet diameter is 430 mm. Fig. 2.a shows the profiles and inlet and outlet angles of the blades on conical surfaces of revolution described by section lines h-h, p-p, q-q, r-r and c-c at 0, 25, 50, 75, and 100 per cent span, respectively. The measurement is performed at six coaxial surfaces (SGL) and five transversal planes (TGL) (Fig. 2.b). At the same location the results have been obtained by using the developed RANS solver.

Because of the complexity of geometry of the annular flow passage in this machine, the results are plotted in terms of the following velocity components (Fig. 3), which are resolved geometrically from the measured axial, radial and tangential components:

V_p – the component parallel to the streamwise grid line on which the measurements is made;
V_n – the component normal to the streamwise grid line on which the measurement is made (i.e. the spanwise component), the outward direction being defined as positive;
V_u – the tangential (whirl) component in the stationary frame of reference;
W_u –the tangential (whirl) component in the relative (rotating) frame of reference.

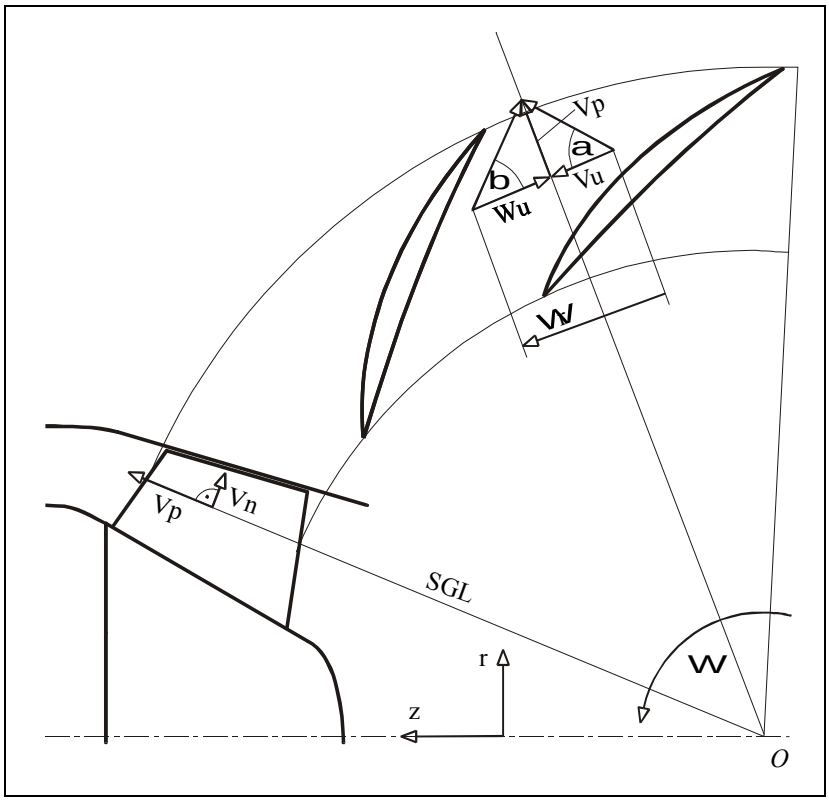

Fig. 3. Description of Velocity Components

Because of the limit of experimental facilities inside the boundary layer it is possible to compare only the values related to the points located at the some distance from the wall. Throughout the presentation of results, all fluid velocities are normalized by the blade velocity at the mid-point of the trailing edge, which is 27 m/s at the 1200 r/min. At the best efficiency point (BEP) the flowrate is 1.01 m^3/s. A grid of 53 x 101 is used for the blade to blade surface with 33 points in the hub to shroud direction (Fig 4.).

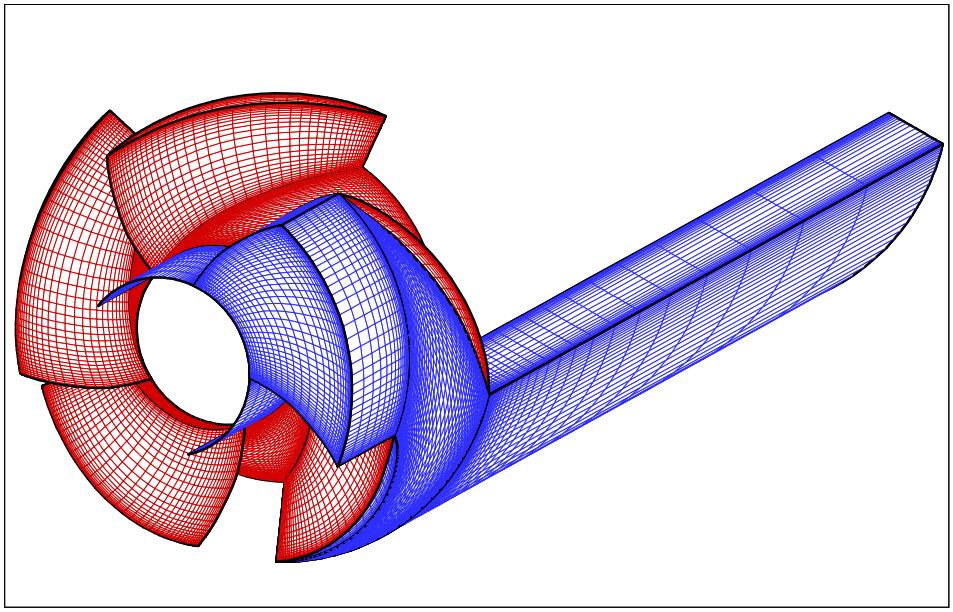

Fig. 4. Computational Grid

The obtained numerical results are in good agreement with the available experimental data in the operating conditions at the best efficiency point (BEP) in the whole region except in a small part of the outer region close to the turbopump casing. In that region the main flow is strongly influenced by the tip leakage that is not considered in this study. Figure 5 shows the blade to blade velocities distributions, both numerical and experimental, from suction to pressure side for mid-span grid line, SGL3. Figure 6 shows passage averaged inlet and outlet relative flow angles, and passage averaged deflection of the flow obtained using numerical model and compared with experimental data.

Also, the turbopump performances are simulated for a number of flow rates and constant shaft speed, corresponding to the off-design operating conditions. The flow rates have been varying from 30% to 110% of BEP flow rate. By decreasing the flow rate the convergence rate of numerical procedure is deteriorated (Fig. 7). Also, at the pump working regimes bellow 50% of BEP flow rates, in outer part of flow field, near to the suction side of blade, the strong flow separation and recirculation, i.e., a backward flow towards the annulus, are noticed (Fig. 8). These phenomena have considerable influence on energy losses at off design operating conditions.

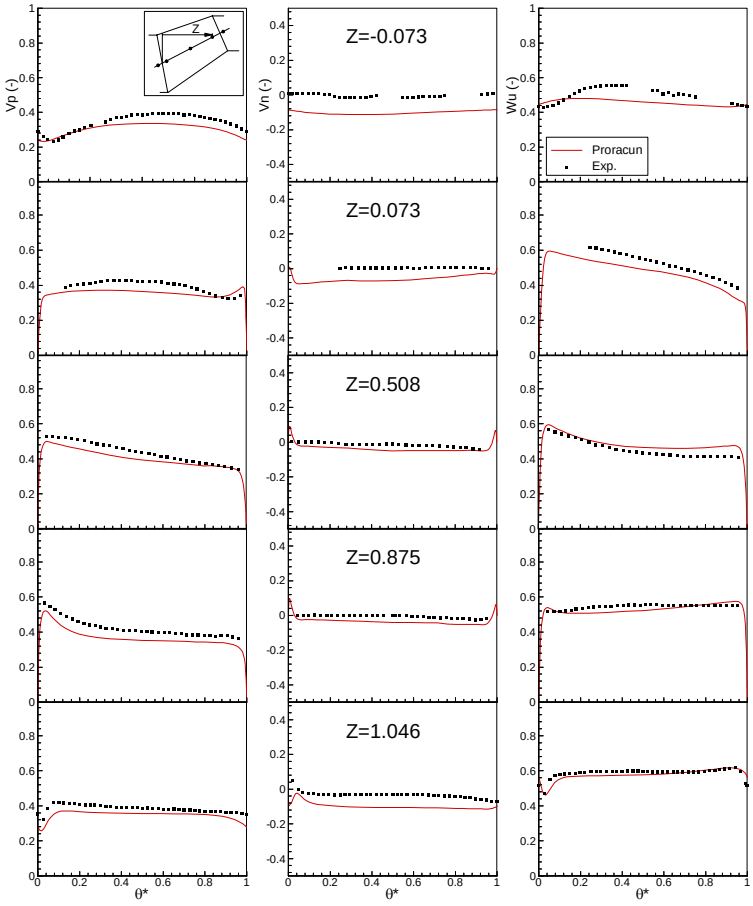

Fig. 5. Blade to Blade Distribution of Velocities on SGL3

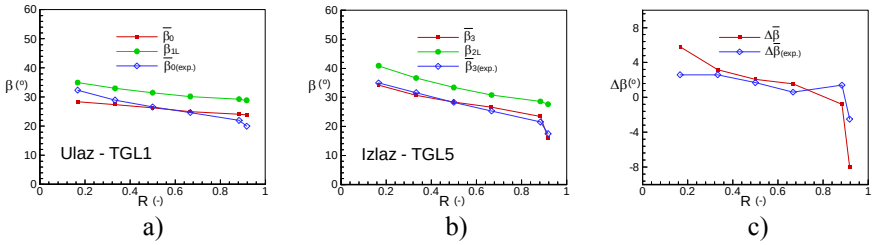

a) b) c)

Fig. 6. Passage Averaged

a) Inlet Relative Flow Angles,
b) Outlet Relative Flow Angles,
c) Flow Deflection.

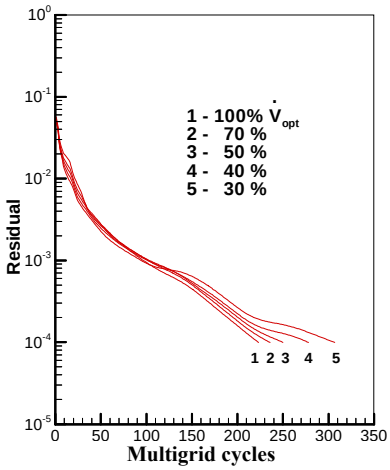

Fig. 7. Convergence History

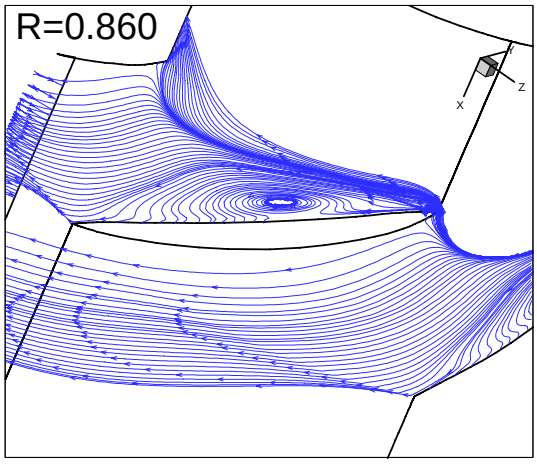

Fig. 8. Streamlines Near the Casing

5. METHODOLOGY FOR DESIGN PERFORMANCE CHARACTERISTICS

According to the information obtained from numerical experiment, in the following text, the methodology for design turbopump performance characteristics (torque, head, powers, and efficiency in terms of flow rates) is shown. The similar procedure for calculation of hydro turbine performance parameters can be found in [23].

Force $d\underset{\sim}{F}^{(i)}$ that acts on an element $dA^{(i)}$ at point C on the $\xi^i = const.$ surface [Fig. 9], in Descartes coordinate can be written as:

$$d\underset{\sim}{F}^{(i)} = dF_{x_1}^{(i)}\underset{\sim}{i}_1 + dF_{x_2}^{(i)}\underset{\sim}{i}_2 + dF_{x_3}^{(i)}\underset{\sim}{i}_3 , \tag{31}$$

where $dF_{x_\alpha}^{(i)}$, $\alpha = (1,2,3)$ are components on the x_α - axis computed from:

$$\begin{aligned} dF_{x_1}^{(i)} &= (-pn_{01}^{(i)} + \tau_{W1}^{(i)})\,dA^{(i)} , \\ dF_{x_2}^{(i)} &= (-pn_{02}^{(i)} + \tau_{W2}^{(i)})\,dA^{(i)} , \\ dF_{x_3}^{(i)} &= (-pn_{03}^{(i)} + \tau_{W3}^{(i)})\,dA^{(i)} . \end{aligned} \tag{32}$$

In equations (32), p is pressure, $\underset{\sim}{\tau}_W^{(i)}$ is wall shear stress vector and $\underset{\sim}{n}_0^{(i)}$ is unit normal vector for element $dA^{(i)}$.

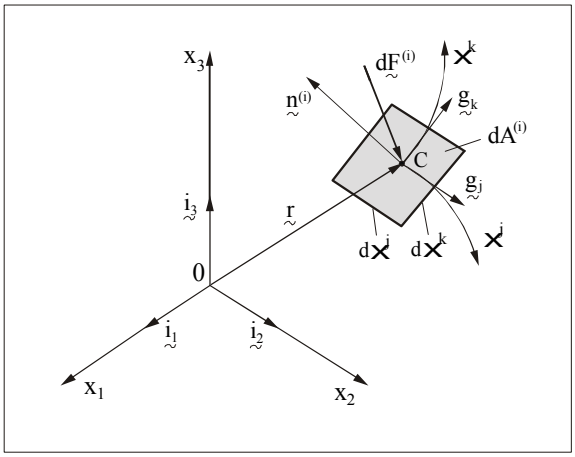

Fig. 9. Computational Element in Global and Local Coordinates

Unit normal vector $\underset{\sim}{n}_0^{(i)}$ can be calculated as:

$$\underset{\sim}{n}_0^{(i)} = \frac{\underset{\sim}{n}^{(i)}}{\left|\underset{\sim}{n}^{(i)}\right|} = \frac{1}{\sqrt{g^{ii}}}(\xi^i_{x_1}\underset{\sim}{i}_1 + \xi^i_{x_2}\underset{\sim}{i}_2 + \xi^i_{x_3}\underset{\sim}{i}_3)\,, \tag{33}$$

where $\xi^i_{x_j}$ are metrics of transformation and g^{ij} are components of contravariant metric tensor. Wall shear stress vector is defined as inner product of stress tensor and unit normal vector, i.e:

$$\underset{\sim}{\tau}_W^{(i)} = \Im \cdot \underset{\sim}{n}_0^{(i)} = \tau_{\alpha\beta}\,\underset{\sim}{i}_\alpha\,\underset{\sim}{i}_\beta \cdot n_{0\gamma}^{(i)}\,\underset{\sim}{i}_\gamma = \tau_{\alpha\beta}\,\underset{\sim}{i}_\alpha\,n_{0\gamma}^{(i)}\,\underset{\sim}{i}_\beta \cdot \underset{\sim}{i}_\gamma = \tau_{\alpha\beta}\,\underset{\sim}{i}_\alpha\,n_{0\gamma}^{(i)}\,\beta_{\beta\gamma}\,, \tag{34}$$

or,

$$\underset{\sim}{\tau}_W^{(i)} = \tau_{\alpha\beta}\,n_{0\beta}^{(i)}\,\underset{\sim}{i}_\alpha = \tau_{1\beta}n_{0\beta}^{(i)}\underset{\sim}{i}_1 + \tau_{2\beta}n_{0\beta}^{(i)}\underset{\sim}{i}_2 + \tau_{3\beta}n_{0\beta}^{(i)}\underset{\sim}{i}_3\,, \tag{35}$$

In relations (34) and (35), $\tau_{\alpha\beta}$, $\alpha\beta = (1,2,3)$ represents Descartes stress tensor components and $\delta_{\beta\gamma}$ is the Kronecker delta.

The fluid torque that acts on an element $dA^{(i)}$ can be written as:

$$d\underset{\sim}{M}^{(i)} = \underset{\sim}{r} \times d\underset{\sim}{F}^{(i)}\,, \tag{36}$$

Torque components around the turbopump axis (x_1) is:

$$dM_{x_1}^{(i)} = x_2\,dF_{x_3}^{(i)} - x_3\,dF_{x_2}^{(i)}\,, \tag{37}$$

Hence, torque that acts on the $\xi^i = const.$ surface may be written as:

$$M_{x_1}^{(i)} = \iint_{A^{(i)}} [x_2 (-pn_{03}^{(i)} + \tau_{w3}^{(i)}) - x_3(-pn_{02}^{(i)} + \tau_{w2}^{(i)})]\, dA^{(i)} , \tag{38}$$

and can be calculated numerically. Assuming that surfaces $j = 1$ and $j = j_m$ denote hub and shroud, and that surface $k = 1$ and $k = k_m$ represent blade pressure and suction side, total torque around the turbopump axis, acts on an impeller passage is:

$$M_{x_1} = M_{x_1(j=1)}^{(2)} + M_{x_1(j=j_m)}^{(2)} + M_{x_1(k=1)}^{(3)} + M_{x_1(k=km)}^{(3)} , \tag{39}$$

Impeller acts on fluid by the same torque but in opposite direction, i.e,

$$M_K = -Z_L M_{x_1} , \tag{40}$$

where Z_L denotes number of blades. During rotation with angular velocity Ω, mechanical power of turbopump impeller is:

$$P_K = \Omega M_K , \tag{41}$$

Hydraulic power can be defined according to the energy balance between inlet ($i = 1$) and outlet ($i = i_m$) of the turbopump:

$$P_H = Z_L \rho [\iint_{A^{(1)}(i=i_m)} (\frac{p}{\rho} + \frac{c^2}{2})(\underset{\sim}{n}_0^{(1)} \cdot \underset{\sim}{c})\, dA^{(1)} - \iint_{A^{(1)}(i=1)} (\frac{p}{\rho} + \frac{c^2}{2})(\underset{\sim}{n}_0^{(1)} \cdot \underset{\sim}{c})\, dA^{(1)}] , \tag{42}$$

Turbopump efficiency represents ratio between output (P_H) and input power (P_K) as:

$$\eta_i = \frac{P_H}{P_K} , \tag{43}$$

Hence, turbopump head is:

$$Y = \frac{P_H}{\rho \dot{V}} , \tag{44}$$

where $\dot{V}$ denotes volume flow (m^3/s).

Dimensionless turbopump characteristics, torque, mechanical and hydraulic power can be written as [24]:

$$M_K^* = \frac{M_K}{\rho U_0^2 L_0^3} , \qquad P_K^* = \frac{P_K}{\rho U_0^3 L_0^2} , \qquad P_H^* = \frac{P_H}{\rho U_0^3 L_0^2} , \tag{45}$$

where L_0 and U_0 represent referent length and velocity, respectively. Dimensionless turbopump head is head coefficient i.e:

$$\psi = \frac{2Y}{U_0^2} \tag{46}$$

Using the numerical procedure presented in this paper, as well as results from the numerical experiment, turbopump dimensionless performance characteristics are designed in term of the flow coefficient (dimensionless volume flow) that is shown in Figure 10.

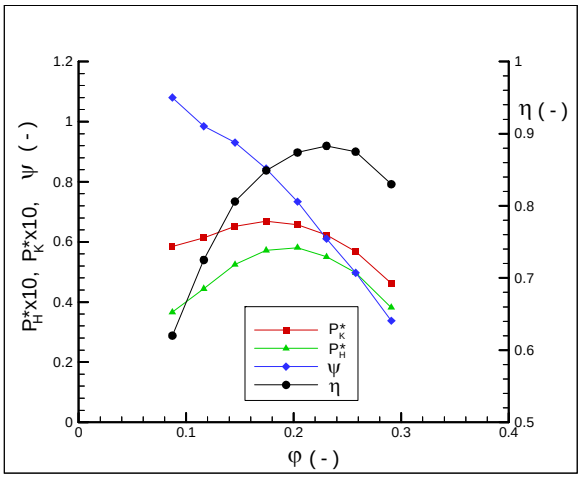

Fig. 10. Turbopump Dimensionless Performance Characteristics

In the regime which is defined by the experiment as a regime at the best efficiency point, the flow coefficient is $\varphi = 0.26$, while the numerical value of the head coefficient is $\psi = 0.5$. Turbopump efficiency obtained by the numerical simulation is 0.88 that is very close to the measured value of efficiency that is 0.87. But, the difference noticed between numerical (192 J/kg) and experimental turbopump head value (202 J/kg) indicates that an appropriate empirical relation should take into account mechanical losses, neglected in numerical algorithm.

6. Conclusion

The developed mathematical model is applied to a model of mixed-flow bowl pump and the numerical solutions for the regime at the best efficiency point, in comparison with the experimental data are reasonable and correctly represent the complex turbomachinery flow phenomena. Also, the turbopump performances are simulated for a number of flow rates and the constant shaft speed, corresponding to the off-design operating conditions. Using information obtained from numerical experiment, methodology for design performance characteristics (head, powers, and efficiency in terms of flow rates) is presented and applied to the turbopump model. By further improvement of the mathematical model, the developed methodology enables that, from an engineer's perspective, numerical experiment could be useful, low-cost tool in comparison with the expensive measurements. Using the dimensionless characteristics as well as theory of conformity, the turbopump performance can be calculated within the wide operating regimes in a relatively simple way. Thus, the turbopump behavior can be predicted very well for all exploitation conditions. These numerical results can be very useful for flow field prediction and presents the basic tool in the high performance turbomachinery design.

REFERENCES

1. C. Hirsch, Numerical computation of internal and external flows, Volume 2: Computational Methods for Inviscid and Viscous Flows, John Wiley & Sons, 1988.
2. N. Kroll, R. Radespiel, C.-C. Rossow, Structured grid solver I, Accurate and efficient flow solver for 3D applications on structured meshes, AGARD - R - 807, 1995.
3. J. Blazek, Investigation of the implicit LU-SSOR scheme, DLR-FB 93-51, 1993.
4. F. B. Lin, F. Sotiropoulos, Strongly-coupled multigrid method for 3-D incompressible flows using near-wall turbulence closures, J. of Fluid Eng., Vol 119, 1997.
5. C. Sheng, L. Taylor, D. Whitfield, A multigrid algorithm for three-dimensional incompressible high Reynolds number turbulent flows, AIAA Paper 94-2335, 1994.
6. X. Zheng, C. Liao, C. Liu, C. H. Sung, T. T. Huang, Multigrid computation of incompressible flows using two-equation turbulence models: Part I-numerical method, J. of Fluid Eng., Vol 119, 1997.
7. A. Jameson, W. Schmidt, E. Turkel, Numerical solutions of the Euler equations by FVM using Runge-Kutta time stepping schemes, AIAA Paper 81 - 1259, 1981.
8. A. Arnone, R. Pacciani, A. Sestini, Multigrid computations of unsteady rotor-stator interaction using the Navier -Stokes equations, J. of Fluid Eng., Vol. 117, 1995.
9. A. Arnone, S. S. Stecco, Multigrid calculation of incompressible flows for turbomachinery applications, XXIV IAHR Congress, Madrid, 1991.
10. R. V. Chima, J. W. Yokota, Numerical analysis of three-dimensional viscous internal flows, AIAA Journal, Vol. 28, No. 5, 1990
11. F. Liu, A. Jameson, Multigrid Navier-Stokes calculations for three-dimensional cascades, AIAA Journal Vol 31, No. 10, 1993
12. J. V. Soulis, An Euler solver for three-dimensional turbomachinery flows, International Journal for Numerical Methods in Fluids, Vol. 20, 1995.
13. C. Carey, S. M. Fraser, D. Rachman, G. Wilson, Studies of the flow of air in a model mixed-flow pump by Laser Doppler Anemometry, NEL Report No. 699, 1985
14. A. J. Chorin, A Numerical method for solving incompressible viscous flow problem, J. of Computational Physics, Vol. 2, 1967
15. J. V. Soulis, N. Jovicic, D. Milovanovic, M. Babic, M. Despotovic, Numerical modeling of incompressible flow in turbomachinery, Computational Fluid Dynamics, Vol 11, pp. 259-265, John Wiley&Sons, 1998
16. D. Wilcox, Simulation of transition with two-equation turbulence model, AIAA Journal, Vol 32, No 2, 1994
17. N.Jovicic, Numerical modeling of incompressible turbomachinery fluid flow, Ph.D thesis, University of Kragujevac,Yugoslavia, 2000
18. M. Zijlema, Computational modeling of turbulent flow in general domains, Ph.D. Thesis, Delft University of Technology, The Netherlands 1996
19. A. Lerat, Une Classe de Schemas aux Differences Implicites Pour les Systemes Hyperboliques de Lois de Conservation, Comptes Rendus Acad. Sciences Paris, Vol. 288 A, 1979.
20. R. C. Swanson, E. Turkel, Multistage schemes with multigrid for Euler and Navier-Stokes Equations, Component and Analyses, NASA TP 3631, 1997
21. F. Menter, Zonal two equation k-ω turbulence models for aerodynamic flows, AIAA Paper, 93-2906, 1993
22. D. Milovanovic, Theoretical and experimental investigation of fluid flow in hydraulic turbomachinery, Ph.D. Thesis, University of Kragujevac, Yugoslavia, 1994.
23. F. Lin, Development of a numerical method for three-dimensional incompressible flow with multigrid acceleration and near-wall turbulence closure, Ph.D. Thesis, University of Iowa, 1996.
24. N. Jovicic, M. Despotovic, Babic M., Milovanovic D., Numerical Simulation of Turbomachinery Fluid Flow, TMT 2002, Neum, B&H, 2002.

SIMULACIJA RADNIH KARAKTERISTIKA HIDRAULIČKIH TURBOMAŠINA

Nebojša Jovičić, Milun Babić, Gordana Jovičić, Dušan Gordić

U ovom radu prikazan je numerički algoritam za simulaciju trodimenzijskog strujanja realnog fluida kroz pokretne i nepokretne lopatične organe hidrauličnih turbomašina. Razvijeni programski paket primenjen je za numeričku analizu radnih procesa u dijagonalnoj turbompumpi. Na osnovu poređenja rezultata proračuna sa postojećim eksperimentalnim podatacima za optimalni režim rada turbopumpe, utvrđen je visok stepen pouzdanosti numeričkog algoritma u većem delu protočnog prostora. Takođe, izvršene su simulacije i detaljna analiza radnih režima pri nižim vrednostima zapreminskog protoka. Prikazana je i metodologija za formiranje radnih karakterisitka turbopumpe (napor, snage i stepen korisnosti u funkciji protoka) na osnovu sprovedenog numeričkog eksperimenta. Izložena metodologija otvara mogućnost da sa daljim razvojem i unapređenjem matematičkog modela, numerički eksperiment obezbedi projektantima informacije do kojih se dolazi isključivo merenjima uz angažovanje skupe opreme.

Ključne reči: *Numerički metod, RANS, dijagonalna pumpa, radne karakteristike*